

Interfacial trapping in an aged discotic liquid crystal semiconductor

Nathan J. Dawson,¹ Michael S. Patrick,¹ Sanjoy Paul,² Brett Ellman,²
 Alexander Semyonov,³ Robert J. Twieg,³ Rachael Matthews,⁴ Emily Pentzer,⁴
 and Kenneth D. Singer¹

¹Department of Physics, Case Western Reserve University, Cleveland, Ohio 44106, USA

²Department of Physics, Kent State University, Kent, Ohio 44240, USA

³Department of Chemistry, Kent State University, Kent, Ohio 44240, USA

⁴Department of Chemistry, Case Western Reserve University, Cleveland, Ohio 44106, USA

(Received 29 March 2015; accepted 17 August 2015; published online 31 August 2015)

This study reports on time-of-flight (TOF) hole mobility measurements in aged 2,3,6,7,10,11-Hexakis(pentyloxy)triphenylene columnar liquid crystals. In contrast to the original samples reported in 2006, homeotropically aligned samples yielded TOF transients with an extended non-exponential rise. The experimental data were fit to a simple model that accurately reproduces the TOF transients assuming delayed charge release from traps near the optically excited electrode. While interfacial trapping appears only in the aged materials, the bulk mobility is similar to the pristine material. The model addresses dispersive transport in quasi-one-dimensional materials, determines the charge carrier mobility in systems with interfacial traps, and provides a method for characterizing the traps. © 2015 AIP Publishing LLC. [<http://dx.doi.org/10.1063/1.4929749>]

I. INTRODUCTION

Charge transport properties of discotic liquid crystals in the homeotropic Col_{ho} phase have been an area of interest over several years because of their potential as easily processed ordered materials.^{1–3} The Col_{ho} phase is observed in 2,3,6,7,10,11-Hexakis(pentyloxy)triphenylene (HAT5) when cooled through the phase transition at 122 °C from the isotropic phase.⁴ The columnar alignment of molecules allows for faster transport of charge carriers compared to disordered systems due to the π - π stacking of the aromatic cores.^{5,6} The photocurrent transients observed in the Col_{ho} mesophase of discogens typically have low dispersion due to the quasi-one-dimensional transport, where the charges are confined to travel along the columns.⁷

Several models have been proposed to describe the physics of charge transport in semiconducting liquid crystals.^{8,9} Work performed in the past suggests that HAT5's transport properties are band-like,⁷ which was described by the small polaron model.^{10,11} Typical mobility measurements for organic semiconductors use techniques such as microwave conductivity^{12–15} for the intrinsic mobility, and space-charge limited current^{16–19} and time-of-flight^{20–23} (TOF) techniques to determine the extrinsic mobility. The TOF technique ideally generates charge carrier sheets from a short absorption depth that travel along the bulk of the sample when applying a bias voltage across the counter electrodes. A transient current is measured as the charge carriers move towards the opposite electrode. Because TOF is an extrinsic measurement of the mobility, the results are most relevant for devices with large domains. The TOF technique also probes traps caused by defects and impurities via the transient behavior that affects the observed temporal photocurrent.^{24,25} Our study focuses on TOF measurements of aged HAT5 between aluminum electrodes. The results of these recent experiments show a delayed increase of the

photocurrent, which is in contrast to the flat photocurrent transients observed a decade ago from *the same synthesized batch* of material. The photogenerated transients showing a delayed release of charge in this paper are under the same experimental conditions as previous experiments conducted on pristine samples of HAT5.

Reports of a delayed release of positive charge carriers into the bulk have previously been reported for triphenylene derivatives.²⁶ Electrode-enhanced hole generation was observed in the smectic B phase of phenylanthracene between platinum electrodes and indium-tin-oxide electrodes; however, enhanced charge generation from aluminum electrodes was found to be negligible.²⁷ The experimental observations and successful reproduction of the photocurrent by the proposed model strongly suggest that there is an interfacial trapping region in the aged HAT5 near the electrode interface that causes the delayed release of holes, which is the experimental focus of the paper. We show how a phenomenological three-state model of an interfacial trapping region reproduces the phototransients and provides accurate bulk mobilities. The model is used to compare the mobilities of the aged HAT5 material with those previously reported, where we show that the bulk material is relatively unchanged with major differences only appearing at the interfacial region. These differences are not due to mechanisms associated with space-charge-limited current.

II. EXPERIMENT

The original HAT5 material was first synthesized by VOCl₃ mediated trimerization of 1,2-bis pentyloxybenzene followed by realkylation.⁷ The purification steps were originally documented by Duzhko *et al.*²⁸ After synthesis 10 years ago, the HAT5 was stored in a closed bottle (under air) and stored in ambient laboratory conditions out of direct light. In order to determine the nature of impurities in the

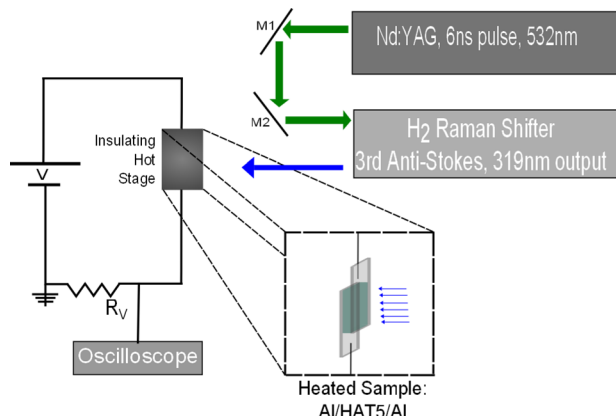


FIG. 1. A Nd:YAG laser pumps a Raman Shifter which excites the HAT5 sample with 6 ns pulse of 319 nm light. The electric field across the sample is applied through the voltage source and the photocurrent collected by the back electrode is terminated across the variable resistor, R_V , and imaged on a Textronix oscilloscope.

aged samples, the decade old HAT5 was dissolved in chloroform and drop-casted onto a target substrate. The sample was then placed in a Bruker Autoflex III Matrix-Assisted Laser Desorption/Ionization Time-of-Flight (MALDI-TOF) mass spectrometer. This method was used to scan for trace levels of impurities.

The charge carrier TOF cells consist of two glass slides with a thin aluminum layer thermally deposited at CWRU's Materials for Opto/Electronics Research and Education (MORE) Center. Mylar spacers were placed between the electrodes with nominal thicknesses of $12.5 \mu\text{m}$. We used a thermal epoxy, OMEGABOND[®] 200, cured at 125°C to seal the electrodes and spacers and to create a sturdy TOF cell of uniform thickness. The separation between the electrodes of each empty cell was calculated from the interference pattern measured with a UV-VIS spectrofluorometer. An encapsulated hot stage heats the TOF cell into the isotropic phase, where we fill the empty TOF cells with HAT5 via the capillary effect. We cooled the HAT5 through the isotropic-Col_{ho} phase transition (122°C) at a rate of $6^\circ\text{C}/\text{h}$ and observed domain formation using polarized light microscopy. The domain structures of the Col_{ho} phase were over $100 \mu\text{m}$ in width ensuring that a single domain spans the much shorter distance between the electrodes. All final sample thicknesses were in the range of $11\text{--}16 \mu\text{m}$, and the semitransparent Al cathodes had thicknesses between 10 and 15 nm.

A Keithley LRC meter measured each cell's resistance and capacitance (at 1 kHz and 10 kHz), which was used to calculate the resistor-capacitor (RC) time constant. As seen in Fig. 1, the TOF setup consists of a current divider circuit where a bias is applied across the sample, pulsed laser light illuminates the sample, and a 2 GHz Tektronix 784D oscilloscope captures the photocurrent transient. The voltage source was a Keithley model 6517A electrometer. A $5 \text{ k}\Omega$ resistance is used as the resistor in the current divider, which is the same value of resistance used by Duzhko *et al.*⁷ Wavelength dependent and pump-delay measurements used a transimpedance amplifier instead of a current divider to record the photocurrent transients with faster response times. The oscilloscope was terminated with a 50Ω resistor in DC mode

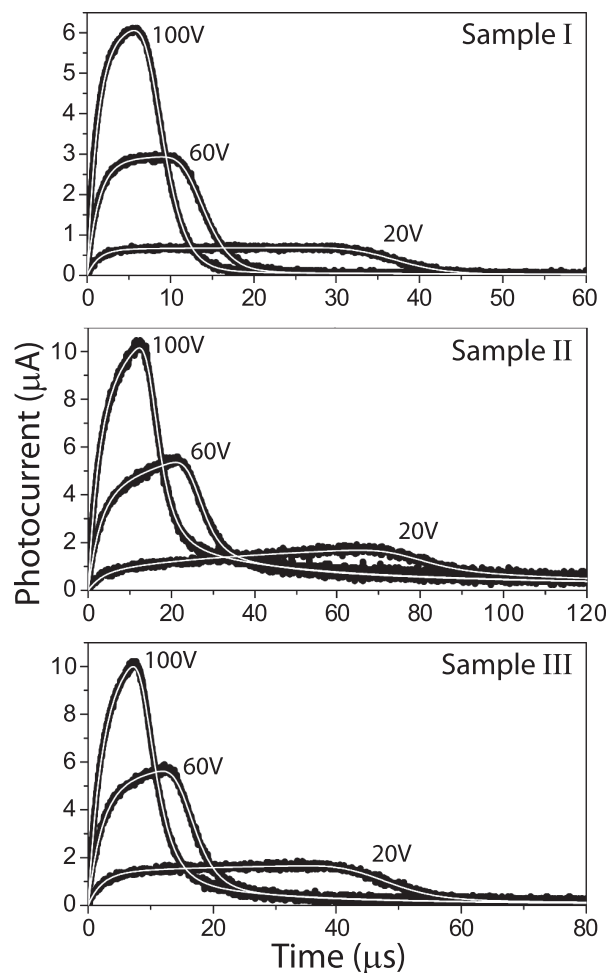


FIG. 2. The photocurrent as a function of time for three different samples at 80°C for various potential differences across the cells. The thick black line is the experimental data and the thin white line is the nonlinear fitted transient from our simple model. Each sample has different trapping characteristics at the interface.

when we used the transimpedance amplifier for short response-time measurements.

Once the material cools below 122°C to form the Col_{ho} phase, the TOF cell is illuminated by pulsed laser light. A 6 ns, frequency doubled, Nd:YAG laser pumps an H₂ Raman shifter. The third anti-Stokes line has a wavelength of 319 nm with a time-average output power of $\sim 10 \mu\text{W}$. Electron-hole pairs are generated in a thin absorption layer near the interface due to the high absorbance of columnar HAT5 at 319 nm.

III. RESULTS

The phototransients from TOF experiments performed on aged HAT5 using the setup shown in Fig. 1 for this study are shown in Fig. 2. The solid black lines are the photocurrents captured by the oscilloscope as a function of time. We observed the delayed rise in the current after an impulse of light for every sample of aged material. This observation is in contrast to previous data taken for HAT5 samples, which were studied shortly after synthesis.⁷ Typical TOF phototransients from this previous study by Duzhko *et al.* are shown in Fig. 3.

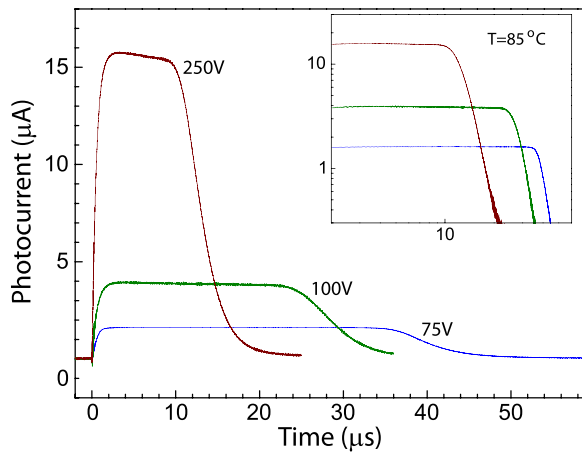


FIG. 3. Photocurrent transients of HAT5 from the year 2006 at applied biases of 75, 100, and 250 V. The inset is a double logarithmic scale of the same transients (after Duzhko *et al.*⁷)

The aged transients never fully plateau; rather, the transients slowly increase in amplitude and continue to release charge into the bulk after the majority of the positive carriers reach the terminating electrode. This slow increase in the induced photocurrent appears as a non-exponential growth as shown in Fig. 8. The longer rise times and lack of a plateau-like region in the transient lead to speculation that the charge carriers are not transiting through the material as a “sheet-of-charge,” which is in contrast to previous studies under similar experimental constraints (Fig. 3) where trapping was found to be negligible.

Despite the delayed injection of positive charge carriers from the interfacial traps into the bulk, the mobilities of the aged HAT5 samples were similar to those found in the previous study by Iino *et al.*²⁹ and Duzhko *et al.*⁷ The results shown in Fig. 3 are typical of the transients obtained by Duzhko *et al.*; however, these results do not represent the fastest mobilities quoted by Duzhko *et al.*⁷ The mobilities are given in Table I, where μ_{S-M} is the mobility calculated via Scher-Montroll method³⁰ and μ_f is the mobility obtained from fitting the model described in Section IV.

The measured ranges of the bulk mobility of the material do not appear to significantly change with age as shown in Table I. The trapping characteristics near the interface, however, change as the material is aged, which is observed by comparing the photocurrent transients in Figs. 2 and 3, where we have shown the latter data from 10 years ago to illustrate the importance of degradation in stock material and the delay of charge entering into the bulk in TOF experiments. The uncertainties in the mobility estimated using either technique are small for each individual sample. The range of mobilities between samples, however, has much larger variations.

TABLE I. Mobility at 85 °C and 100 V ($\times 10^{-3}$ cm² V⁻¹ s⁻¹).

Study	Samples	μ_{S-M}	μ_f
2006	From Duzhko <i>et al.</i> ⁷	0.7 – 2.0	—
2014	I	2.17 ± 0.01	1.93 ± < 0.01
	II	1.48 ± 0.01	1.44 ± < 0.01
	III	1.86 ± 0.01	1.75 ± < 0.01

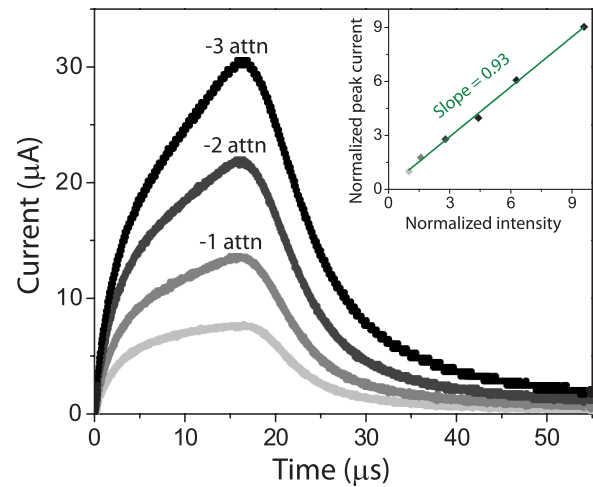


FIG. 4. The transient of a typical sample at varying intensities.

We found that the interfacial characteristics change in both the original fabricated TOF cells and those newly created from the bulk container of aged HAT5. Note that HAT5 is in the crystalline phase when stored inside a TOF cell at room temperature, whereas every sample (an original cell or newly created one) was heated into the isotropic phase and slowly cooled into the Col_{h0} phase prior to each new measurement.

The intensity dependence was measured by removing glass attenuators (attn) between the Raman cell and the sample at 319 nm. The attenuators were 2 mm thick with a measured transmittance of 58% at 319 nm. The transients shown in Fig. 4 (at 80 °C and 39.6 kV/cm) are not representative of a sample illuminated to the extent that the presence of free charges generated by a light source (or repeated illumination at 10 Hz) causes significant changes to the local fields. Furthermore, the peak photocurrent has a linear relationship with respect to the pump intensity upon incrementally attenuation and results in a 93% slope, which also affirms that we are not observing space-charge-limited current.

Additional variations of the TOF experiment were performed to elucidate how interfacial trapping caused the delayed release of charge in aged HAT5. The plot in Fig. 5(a) shows transients for the same TOF cell excited by either a 319 nm or a 355 nm source. The longer pump wavelength causes the absorption length to increase, where the aged HAT5 begins to resemble the shape of the photocurrent transients in the pristine samples. The inset of Fig. 5(a) shows a segment of the UV absorption curve of a thin film of HAT5 spin coated from chloroform and heated to 100 °C for 20 min, where the source wavelengths of 319 nm and 355 nm have been marked. The long-time peaks of the photocurrents have been scaled in arbitrary units to provide a clear comparison. We can relate the delayed release of charge carriers to the penetration depth of the exciting field via the Beer-Lambert law, which is applicable when far from saturable absorption. The absorption coefficient at 319 nm is much larger than at 355 nm. The initial sharp rise in photocurrent after a sample pumped at a wavelength of 355 nm is large relative to the peak value, which is in contrast to the photocurrent from the same sample pumped at 319 nm. Because

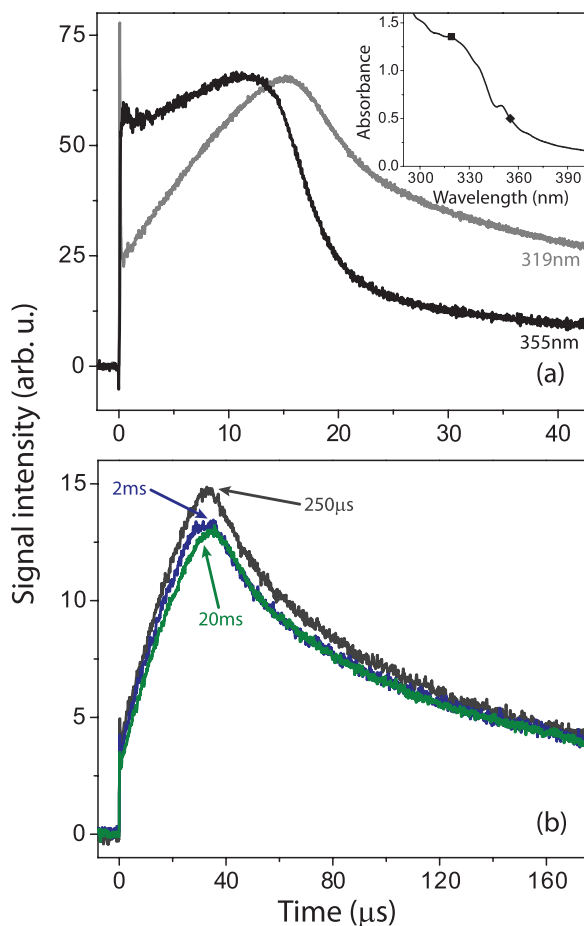


FIG. 5. (a) Two transients of the same TOF cell and at the same voltage, where the pump wavelength is changed between 319 nm and 355 nm. The inset shows a portion of the UV absorption spectrum for aged HAT5 dissolved in chloroform and spin coated on a glass substrate. The pump wavelengths are marked with black diamonds. (b) The photocurrent transient of an aged HAT5 sample as a function of pump delay between the onset of a voltage bias and the 319 nm light pulse.

the sharp rise after the initial 319 nm pulse is much smaller than the sharp rise in photocurrent after the pulse at 355 nm, a much greater number of charges are delayed when pumped at 319 nm. Thus, the degree to which the excitation at the higher wavelength lowers the amount of initially trapped charges is further evidence that there is significant charge trapping that occurs near the HAT5/electrode interface.

The other TOF experiment performed for characterization utilized a delayed photogeneration technique after the work by Pokhrel *et al.*^{23,31} Here, any ions in the sample are allowed to thermally diffuse in the absence of a voltage to reach a net charge-neutral state. The TOF voltage is then applied and the laser is triggered at a specified delay time after the ions begin drifting under the applied field. Therefore, the concentration of ions at each electrode is a function of delay time. Note that the mobility of ions in the discotic is expected to be much smaller than that of the holes; therefore, the ionic configuration is essentially constant as the holes traverse the sample. Three transients are shown in Fig. 5(b), where the data sets have a pulse delay time that is separated by an order-of-magnitude. We did not observe any change in the shape of the transient as the pulse delay is increased.

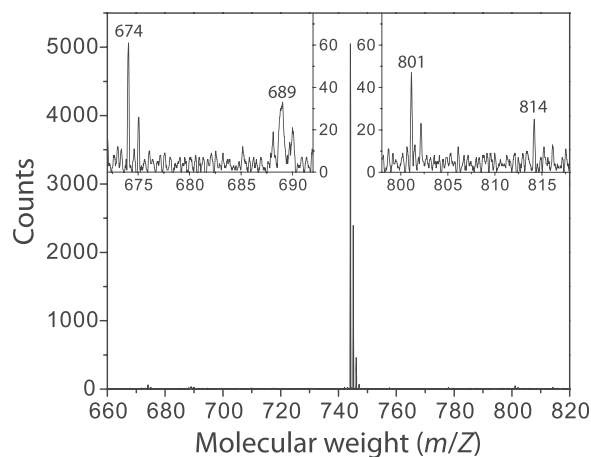


FIG. 6. MALDI-TOF from a sample of aged HAT5. The insets show the molecular weights for impurities that can be measurement above the noise.

Thus, we suspect that mobile ion/carrier build-up at the interface is not responsible for the observed interfacial traps.

As shown in Fig. 6, we observed a few contaminant lines using the MALDI-TOF apparatus, which registered around 1% of the peak signal from the HAT5 line at 744 m/Z . Either one or a combination of these impurities shown in Fig. 6 might be the cause of the interfacial traps. The line at 674 m/Z likely corresponds to a missing pentyl chain from a degraded species of HAT5. The fragments located above 800 mass ratio are unknown. Thus, the drastic change in the transients from TOF experiments from a small impurity emphasizes the TOF method as a sensitive measurement for the purity of a discotic liquid crystal semiconductor.³²

IV. THEORY

In this section, we model the transient in order to explain the slow rise and decay of the photocurrent. We begin with the continuity equation of charge carriers derived from the Boltzmann equation and make simplifying assumptions about the nature of trapping in a columnar liquid crystal with quasi-one-dimensional transport. There have been significant contributions in describing the behavior of photocurrent transients from the trapping and release of charge carriers.^{25,33–37} In the present work, we make note of the lack of permanent traps in the pristine HAT5 and the apparent lack of any significant trapping of charge carriers in the bulk of the aged material when increasing the penetration depth of the pump. Thus, we formulate a simple one-dimensional transport model with only interfacial trapping.

The continuity equation for both positive and negative charge carriers may be written as

$$\mp \nabla \cdot \mathbf{J}_{\pm}(x, y, z, t) + \frac{\partial \rho_{\pm}(x, y, z, t)}{\partial t} = \mathcal{S}_{\pm}(\rho, x, y, z, t), \quad (1)$$

where \mathbf{J} is the current density, ρ is the charge carrier distribution, and \mathcal{S} is the net charge generation/recombination term. The \pm subscripts denote either holes (+) or electrons (–). Charge transport in the plane perpendicular to the optical axis is negligible because these TOF cells are much thinner

than the laser's spot size and the carriers are mostly confined to travel along the electric field lines (which also corresponds to the orientation of the columns in the liquid crystal). Therefore, Eq. (1) simplifies to the one-dimensional continuity equation

$$\mp \frac{\partial J_{\pm}(x, t)}{\partial x} + \frac{\partial \rho_{\pm}(x, t)}{\partial t} = \mathcal{S}_{\pm}(x, t). \quad (2)$$

The scalar current density is related to the drift mobility and diffusivity by the equation

$$J_{\pm}(x, t) = \rho_{\pm} \mu_{\pm}(\rho_{\pm}) E(x, t) + D_{\pm} \frac{\partial \rho_{\pm}(x, t)}{\partial x}, \quad (3)$$

where $\mu(\rho)$ is the dispersive drift mobility, E is the electric field, and D is the carrier diffusivity. For strong enough applied fields over short time scales, the first term due to drift on the right-hand-side of Eq. (3) dominates and, therefore,

$$J_{\pm}(x, t) \approx \rho_{\pm} \mu_{\pm}(\rho_{\pm}) E(x, t). \quad (4)$$

The electric field from the presence of free charges in the material can be expressed by the Poisson equation

$$\nabla \cdot [\epsilon \nabla V_c(x, t)] = \rho(x, t), \quad (5)$$

where V_c is the scalar electric potential due to free charges in the material and ϵ is the tensor component of the linear permittivity along the direction of columnar stacking. The incident intensity was kept low to avoid space-charge limited transport for the range of fields used in the hole transport TOF experiments.³¹

We illuminate at the cathode interface, where the majority of charge pair generation takes place due to the high absorbance of the material at 319 nm. Because the electron's transit time to the illuminated electrode is faster than the RC-time constant, we no longer consider a time-resolved electron transport equation. Henceforth, we remove all \pm subscripts and only consider hole transport.

We assume a narrow Gaussian Mobility Distribution Function (MDF),^{38,39} where we solve the drift equation over a discrete set of mobilities and normally distribute the calculated current amplitudes. Note that other methods that consider the density-of-states function for charge transport have been used to characterize dispersive, multi-dimensional transport in disordered media,⁴⁰⁻⁴³ including the multi-trapping model for smectic phenylanthracene derivatives with trapping at the material boundary.⁴⁴

Due to the slow (significantly longer than the circuit's response time), non-exponential, increase of the current in response to an incident light pulse, we propose a mechanism for the delayed release of charge. Previous work has described delayed charge injection in phenylanthracene with indium-tin-oxide and platinum electrodes.²⁷ We observed the same non-exponential current growth for our samples with aluminum electrodes created in both nitrogen atmosphere and oxygen rich environments, indicating that aluminum oxide is not a factor. In addition, hole injection directly from the aluminum electrodes is energetically unfavorable. Thus, the most probable scenario for the observed

delayed release of holes into the bulk is due to trapping in the illuminated region near/at the cathode/HAT5 interface. This is similar to past results for delayed charge carrier release in polyethylene;⁴⁵ however, the quasi-one-dimensional nature of HAT5 makes it unlikely that there is a redistribution of charges along an interfacial barrier.

Because the mobilities between the pristine and aged samples are similar, there are no additional low-energy traps in the bulk that increase the transit time from any additional trapping and releasing of carriers. Also, because the shape of the transients in the aged HAT5 approach those of the pristine material when the penetration depth of light is increased, then we assume that there is no additional deep/permanent trapping of the charge carriers in the bulk. Thus, the only trapping region we address is from low-energy traps near the interface. A simple, many-charge-carrier model at the interface may be derived from a set of rate equations for a three-state model, which is similar to those introduced by Van de Walle⁴⁶ to describe hydrogen relaxation in amorphous silicon. This model produces a non-exponential growth in the photocurrent response. The model also describes all photocurrent transients observed in aged HAT5, where it does not make use of the multi-trapping model with a distribution near the interface and two types of trapping near the interface.³⁶

The rate equation for a quantity of holes in a trap near the cathode interface is given by

$$\frac{dN_t}{dt} = -v_t N_t + \sigma_t N_t (M_t - N_t), \quad (6)$$

where v_t is the average rate at which holes are released from the interfacial traps and σ_t is the average collection rate of the interfacial traps. The second term in Eq. (6) depends on the number of holes that are in the intermediate states, N_t , as well as the difference between the number of trapped holes, N_t , and the number of total trapping states, M_t . A diagram of the energies associated with the trapping states, intermediate states, and bulk reservoir is shown in Fig. 7.

The rate equation for the number of holes entering the bulk reservoir is

$$\frac{dN_r}{dt} = -v_r N_r + \sigma_r N_t (M_r - N_r), \quad (7)$$

where the subscript r labels the average release and collection rates associated with the bulk reservoir. The sum of the number of holes generated in the trapping region of the interface is equal to a constant

$$N_r + N_t + N_I \approx N_{i0}. \quad (8)$$

Note that we approximate the total number of holes in the system (only those relevant carriers generated near the interfacial trapping region), N_{i0} , to be constant. This approximation holds when the time scale for initial pair generation/recombination is much less than the time scale for holes to be released into the bulk from the interfacial traps.

In-line with Van de Walle, we first assume that the trapping rate equation occurs on a much faster time scale than

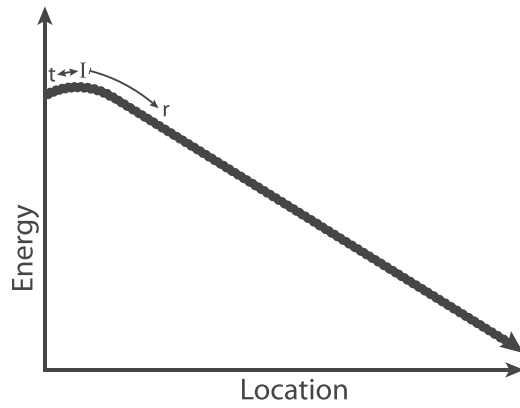


FIG. 7. An illustration of the potential energy in the TOF cell when an electric potential difference is applied across the electrodes. We have labeled the regions for interfacial trapping sites (t), intermediate states (I), and the bulk reservoir (r).

the bulk rate equation. If we also assume that there are only a small number of intermediate states, then the intermediate states are quickly saturated. Therefore, $dN_I/dt \approx 0$, which gives

$$N_I \approx \frac{v_t}{\sigma_t} \frac{N_t}{M_t - N_t}. \quad (9)$$

Substituting Eq. (9) into Eq. (7) gives

$$\frac{dN_r}{dt} = -v_r N_r - \frac{\sigma_r v_t}{\sigma_t} (M_r - N_r) \frac{N_t}{N_t - M_t}. \quad (10)$$

We may also make the assumption that $M_t \gg N_t \gg N_I$, which holds for times that are not exceptionally long such that N_t is reduced to the same order of magnitude as N_r . Then, we may add a small number, N_I , to the numerator and denominator of Eq. (10), where

$$\frac{dN_r}{dt} \approx -v_r N_r - \frac{\sigma_r v_t}{\sigma_t} (M_r - N_r) \frac{N_t + N_I}{N_t - M_t + N_I}. \quad (11)$$

Using the relationship from Eq. (8), we can rewrite Eq. (11) as

$$\frac{dN_r}{dt} = -v_r N_r + \frac{\sigma_r v_t}{\sigma_t} (M_r - N_r) \frac{N_{i0} - N_r}{M_t + N_r - N_{i0}}. \quad (12)$$

We can then normalize the rate equation for hole transfer between the bulk and intermediate states by defining $\mathcal{N}_r = N_r/N_{i0}$, $\mathcal{M}_r = M_r/N_{i0}$, and $\mathcal{M}_t = M_t/N_{i0}$. Substituting these variables into Eq. (12) gives

$$\frac{d\mathcal{N}_r}{dt} = -v_r \mathcal{N}_r + \frac{\sigma_r v_t}{\sigma_t} (\mathcal{M}_r - \mathcal{N}_r) \frac{1 - \mathcal{N}_r}{\mathcal{M}_t + \mathcal{N}_r - 1}. \quad (13)$$

Once the holes enter the bulk, they are carried along the field lines towards the back electrode. Thus, we may simplify Eq. (13) by setting $v_r = 0$. In addition, the number of bulk states is far greater than the number of holes generated in the sample, $M_r \gg N_{i0}$, where it also follows that $M_r \gg N_r$. Thus, only the M_r term in the parentheses for the last term on the right-hand-side makes a significant contribution. Therefore, Eq. (13) reduces to

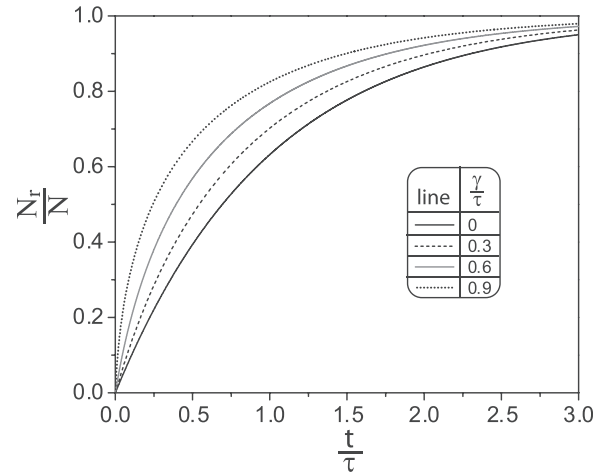


FIG. 8. The increase of holes released to the bulk from interfacial traps as a function of time.

$$\frac{d\mathcal{N}_r}{dt} = \frac{\sigma_r v_t}{\sigma_t} \mathcal{M}_r \frac{1 - \mathcal{N}_r}{\mathcal{M}_t + \mathcal{N}_r - 1}. \quad (14)$$

We then integrate Eq. (14), where the last assumptions allow us to set the initial condition as $\mathcal{N}_r(t=0) = 0$, which gives

$$t = -\frac{\sigma_t}{\sigma_r v_t \mathcal{M}_r} [\mathcal{N}_r + \mathcal{M}_t \ln(1 - \mathcal{N}_r)]. \quad (15)$$

Revisiting our previous statement in which N_{i0} represents all relevant positive charge carriers in the three-state model, the initial condition requires that the total number of relevant holes is in the interfacial trapping region and intermediate states. Although there are also charge carriers generated beyond the interfacial trapping region, the previous simplifying assumptions that $v_r = 0$ and $N_{i0} \ll M_r$ make these charges irrelevant in the three state interfacial trapping model. Note that the initially untrapped charges are important in the context of charge transport because they contribute to the measured photocurrent.

Making the substitutions $\tau = M_t \sigma_t / (M_r \sigma_r v_t)$ and $\gamma = \tau N_{i0} / M_t$, we solve Eq. (15) for \mathcal{N}_r giving

$$\mathcal{N}_r = N_{i0} \left[1 + \frac{\tau}{\gamma} \mathcal{W}(\vartheta) \right], \quad (16)$$

where \mathcal{W} is the zero-root Lambert W function⁴⁷ and

$$\vartheta = -\frac{\gamma}{\tau} e^{-\frac{t+\gamma}{\tau}}. \quad (17)$$

The growth of N_r as a function of time for several values of the stretching/delay time constant γ is shown in Fig. 8.

The source term in the continuity equation, Eq. (2), is the rate at which the hole concentration is released into the bulk over time. If we multiply Eq. (16) by the absolute value of an electron's charge and divide by the volume, then the time derivative gives

$$\frac{d\rho_s}{dt} = -\frac{\rho_{s0}}{\gamma} \frac{\mathcal{W}(\vartheta)}{1 + \mathcal{W}(\vartheta)}. \quad (18)$$

With these approximations and assumptions, and under the aforementioned experimental conditions, the advection of

holes with delayed interfacial trapping may be modeled using the equation

$$\frac{\partial \rho(x)}{\partial t} = \frac{\partial J}{\partial x} - \frac{\rho_{s0}}{\gamma} \int dx \delta(x) \frac{\mathcal{W}(\vartheta)}{1 + \mathcal{W}(\vartheta)}. \quad (19)$$

As previously mentioned, only a fraction of the total charge carriers generated in the illuminated region resides in the nanoscopic trapping region near the electrode interface. The initial condition has a concentration of holes already in the bulk at $t = 0$. Because the nanoscopic scale of charge trapping near the interface is on a much smaller scale than the length increments necessary to model the propagation of holes in the bulk, we set this initial untrapped charge at $x \approx 0$ in the continuity equation

$$\rho(x, t = 0) = \int dx \rho_0 \delta(x). \quad (20)$$

The current density modeled using this method is the true current density signal, provided there is no strong influence from the measurement apparatus on the charge density. Due to the experimental requirements, the capacitance of the TOF cell and the small resistor in the current divider limit the measurement response time (large resistor is the 1 M Ω input impedance of the oscilloscope in AC mode when we used the current divider from Duzhko *et al.*⁷). The RC time constant of the response function varies between samples due to the changes in capacitance with typical values between 1 and 2 μ s. The measured current I_m as a function of the signal current I is given by

$$I_m = \frac{1}{RC} \int_{-\infty}^t dt' I(t') e^{-\frac{t-t'}{RC}}. \quad (21)$$

V. DISCUSSION

A. Numerical method

We approximated the drift equation, Eq. (19), numerically using finite differences via the first-order accurate upwind (upstream) scheme.^{48,49} The first-order accurate scheme was chosen over the second-order accurate scheme due to the dispersion in the material and the negligible depletion of holes recorded in the experiments. Thus, the first-order, upwind, finite-difference method is a suitable approach for approximating the measured photocurrent without depleting the calculated signal. We selected the temporal and spatial steps such that the numerical dispersion was small for the range of mobilities, where there was a small change in the fourth significant figure of the parameters for an order of magnitude change in the time step. A Levenberg-Marquardt nonlinear fitting routine was used to fit the model's output to the experimental data. The theory has six parameters (ρ_{s0} , ρ_0 , τ , γ , μ , σ_μ) that are allowed to vary within a specified parameter range to find the best fit to the photocurrent transients. Fortunately, we were able to limit the fits to only these six parameters due to the simplicity of the model; however, the still large number of parameters and the simple shape of the transients force some parameters to have larger

uncertainties than others. Three TOF samples with differing transient characteristics were analyzed using this theory with a nonlinear fitting routine. Sample III was chosen to study the majority of the interfacial trapping influences due to the prominent features in the transients.

The Lambert W function must be solved for every time step. The calculation of the zeroth-root Lambert W is time consuming for small arguments. The negative fraction multiplied by the delayed exponential in the argument, however, limits the range in which we seek a solution, where the argument is restricted to $(-1/e, 0)$. In this case, we calculate and store the Lambert W values for arguments out to the fifth decimal place. Then, we call these stored values based on the possible input range rounded out to the fifth significant figure. Using this method of approximating the Lambert W function, we reduce the computation time of a nonlinear fitting routine on average by orders of magnitude.⁵⁰

Table II shows the values for the fitted parameters with uncertainties for Sample III at 80 °C. The values given are also found in Figs. 9–11. The uncertainty for the most robust parameters, μ and σ_μ , was obtained from (1) the covariance matrix and (2) calculating parameter sets over several initial guesses. The latter procedure gave a standard error from a set of values for each parameter, where the sets of values used were taken from calculations with the lowest sums of residuals. For the other four parameters (n_0 , n_{s0} , γ , τ), the sensitivity to the variance of the residual was such that unreasonable confidence intervals were obtained. Thus, we estimated the uncertainties from the standard error using the latter and computationally expensive technique.

B. Transients

The ideal transient response for a photogenerated sheet of non-interacting holes that move through a conductive medium and under the influence of an applied electric field should give a box-like phototransient with respect to time. Typically, the photocurrent is not very box-like due to the charge sheet undergoing dispersive effects such as the trapping of charges, loss of charges in deep traps, the spreading of the sheet due to local space-charge effects, and others such as delayed charge injection.

The transit times of dispersive transients are often measured using the Scher-Montroll “knee” method.³⁰ In our case, we assume little dispersion due to trapping and determined the mobility directly from a nonlinear fit to transients, where Fig. 2 shows the fits to experimental data using the model described in this paper. The theory fits exceptionally well for the photocurrent transients in aged HAT5.

C. Mobility and MDF width

We analyzed the data from sample III in Fig. 2 using a nonlinear fitting routine to extract the mobility as a function of temperature and electric field. The mobility is plotted in Fig. 9(a) as a function of temperature over a 100 V range. Note that when applying an electric potential difference of greater than 120 V (for samples 10–20 μ m thick), the circuit typically shorted and degraded the samples during the measurement procedure. The mobility of sample III had the same

TABLE II. Sample III's parameters at 80 °C.

Voltage (V)	$n_0 (\times 10^8)$	$n_{s0} (\times 10^8)$	$\tau (\mu\text{s})$	$\gamma (\mu\text{s})$	$\mu (\times 10^{-3} \text{ cm}^2 \text{ V}^{-1} \text{ s}^{-1})$	$\sigma_\mu (\times 10^{-3} \text{ cm}^2 \text{ V}^{-1} \text{ s}^{-1})$
20	3.62 ± 0.05	1.71 ± 0.10	105.0 ± 11.3	97.4 ± 15.6	1.709 ± 0.001	0.120 ± 0.002
40	3.88 ± 0.12	1.98 ± 0.07	56.6 ± 8.8	50.3 ± 9.1	1.725 ± 0.002	0.128 ± 0.004
60	4.25 ± 0.09	2.09 ± 0.07	55.0 ± 12.5	49.1 ± 8.3	1.733 ± 0.002	0.166 ± 0.003
80	4.44 ± 0.11	2.20 ± 0.12	52.4 ± 8.7	48.6 ± 10.2	1.735 ± 0.003	0.219 ± 0.005
100	4.87 ± 0.09	2.45 ± 0.09	50.6 ± 10.8	43.5 ± 11.6	1.743 ± 0.003	0.217 ± 0.004
120	4.90 ± 0.10	2.43 ± 0.07	48.2 ± 7.0	41.1 ± 5.9	1.761 ± 0.003	0.243 ± 0.003

temperature and electric field dependencies as the other samples with non-negligible interfacial trapping. Note that the mobility increased with electric field for samples with a small number of initially trapped charges (sample I) relative to samples with large interfacial traps (samples II and III), which can be observed from the analysis of the transients shown in Fig. 2.

The Gaussian width, σ_μ , of the MDF at high temperatures increases as the electric potential difference between the two electrodes increases. This increase is shown in Fig. 9(b). If diffusion was the dominant mechanism at high temperatures instead of a drift mobility distribution, then we would expect the calculated Gaussian width of the MDF to decrease as the applied voltage increased. The shape of a

transient's tail due to Gaussian distribution of mobilities looks similar to that caused by the diffusion/repulsion of charge carriers. We could not model both diffusion and an MDF together because they similarly affect the measured photocurrent transients, where large uncertainties arise between these two parameter values due to the indistinguishability between the two mechanisms. We observe a convergence point in the electric field dependence of the MDF's Gaussian width as the temperatures increased, where there is a crossing of the slopes at high temperatures over the voltage range. We interpret this intersection as the system being near the diffusion limit for the transit time scales because (1) there is a reduction in the applied electric field as the voltage is decreased and (2) the order of the liquid crystal system decreases, which causes the mobility to decrease.

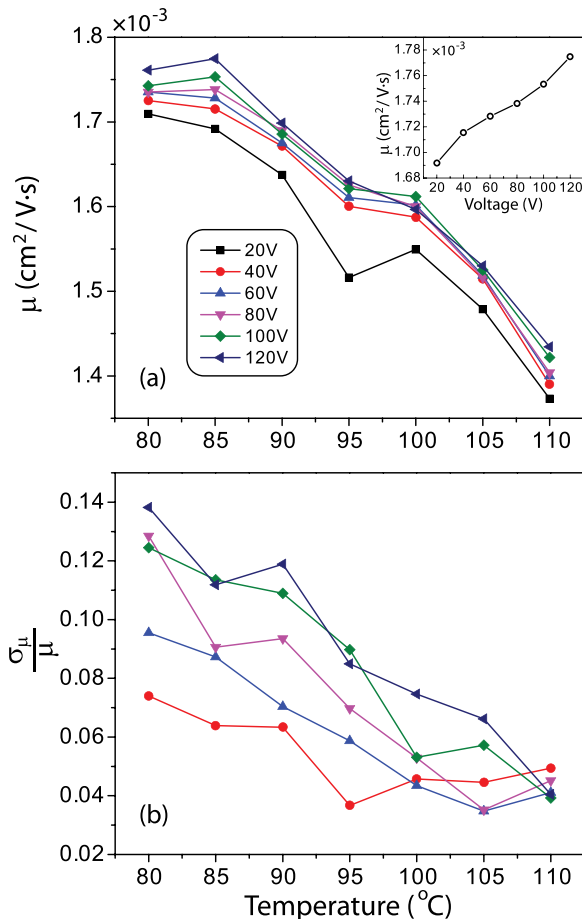


FIG. 9. (a) The mobility and (b) the Gaussian width of the MDF divided by the mobility as a function of temperature and applied voltage across sample III, where the legend represents the data shown in both graphs. The inset in (a) shows the electric field dependence of the mobility 85 °C.

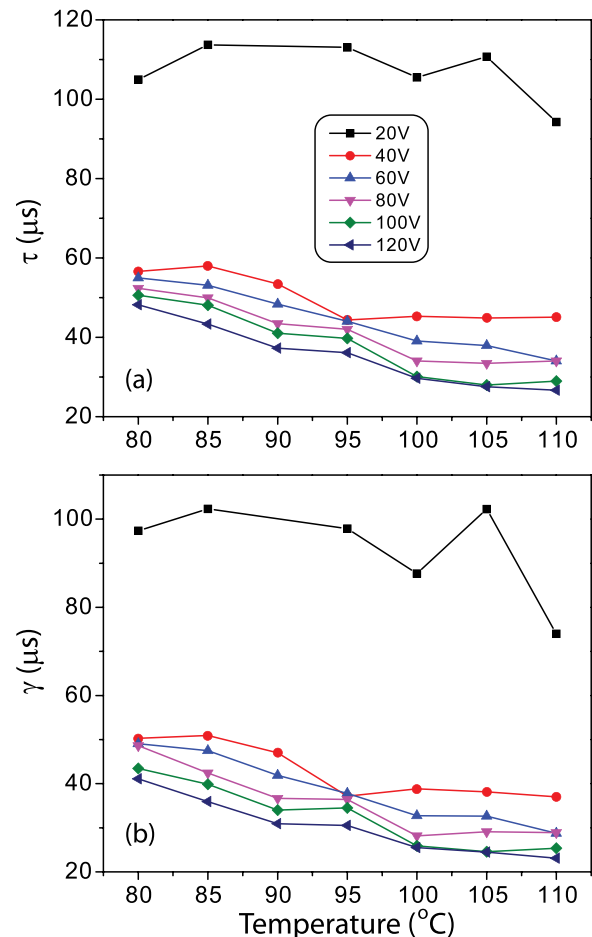


FIG. 10. (a) The exponential growth constant τ and (b) the stretching/delay constant γ as a function of temperature and applied voltage across sample III.

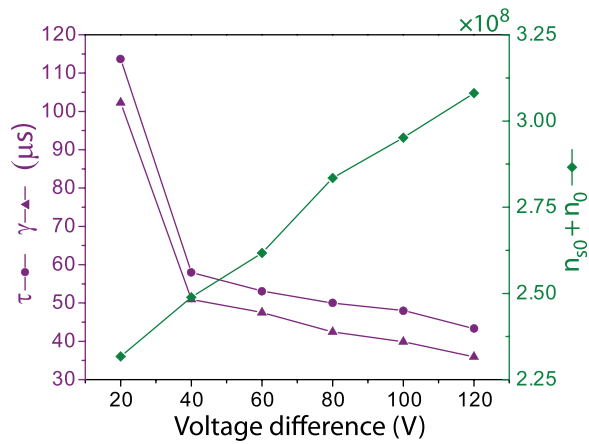


FIG. 11. Sample III's electric field dependencies for τ , γ (left axis) and the total number of holes collected (right axis) at 85 °C.

D. Time constants

The initial trapping at the interface was shown to exhibit a delayed release due to competition between the interfacial traps and intermediate states. Experimentally, we observe that the time constants change between the sample tested, and therefore the collection/release constants are also different between samples. Thus, we may assume that the trap energy at the interface is different between samples. Note that there was always some interfacial trapping for every aged HAT5 cell studied. In addition, since we found that aluminum-oxide plays no role, we may assume the dominant mechanism behind the interfacial trapping parameters originates from impurities in the aged HAT5 material.

The rise and tail shapes in the photocurrent transients are both necessary to find the time constants. The fraction of charge carriers in the bulk to those initially trapped is also most accurately determined when including a long portion of the tail in the nonlinear fitting scheme. The time constant τ is the exponential time constant. If we force $\gamma \rightarrow 0$, then higher values of τ are associated with a faster depletion of trapped charges at the interface, where the Lambert W function in Eq. (16) limits to a negative exponential function for $\gamma = 0$. This limiting case of exponential growth is shown in Fig. 8 for $\gamma/\tau = 0$ (solid black line).

The temperature and field dependencies for τ are shown in Fig. 10(a) for sample III. The values for τ appear to stay relatively constant as a function of temperature. The values for the time constant appear to decrease as the applied voltage increases, where a sharp decrease in the time constant is seen between 20 V and 40 V as shown in Fig. 11. One cause may be that the increased voltage reduces the width of the region where intermediate states exist, i.e., sharpening the cusp in the line representing the voltage as a function of distance. This would increase the probability of bulk collection of holes as a function of voltage. Increasing the voltage may also decrease τ by decreasing the depth of the trap, and thereby increase the rate at which holes are released from the trap and decrease the rate of collection. Also, discogens with a conjugated core in the hexagonal columnar phase undergo a slow homogeneous alignment when a DC voltage is applied.⁵¹ The same effect was observed by us for HAT5

under a polarizing microscope when a large field was applied over a long period of time, and small changes in alignment over a short time scale could affect the differences between the interface and bulk ordering, which may also have some effect on τ 's voltage dependence.

The stretching/delay constant γ follows a temperature and electric field dependence similar to that of τ as shown in Figs. 10(b) and 11. This is not surprising as the fraction γ/τ is associated with the perturbation of Eq. (16) from a common exponential growth function via the product-logarithmic relationship of charge carriers released in the bulk. As previously mentioned, the uncertainty is largest for the time constant parameters when performing a nonlinear fit. Therefore, there is no identifiable trend for the fraction of the time constants γ/τ that can be addressed in this paper. If there is a temperature or electric field dependence on γ/τ , then we expect it to have a small slope.

The total number of holes collected, $n_{s0} + n_0$, follows the opposing progression as shown in Fig. 11. This phenomenon is caused by the increased slope of the potential, where all the charges generated in the bulk are more likely to separate (roughly 2/3 of the total charges generated were in the bulk for sample III), and thereby lower the probability of pair recombination.

E. Size of the interfacial trap region

An essential feature of this model is the ability to calculate the extent of the trapping region of a particular sample. The ability to distinguish the average physical length of the interfacial trapping region is helpful because it can give insights into the degree in which the transients are affected between samples. The first step in finding the trapping region extent is by comparing the fraction of charge density generated in the interface regime normalized to the charge density generated throughout the whole sample. The same step can be done with the charges generated within the bulk as well. The initially trapped charge density, ρ_{s0} , is generated in the region $0 < x < d$, where d is the average length of the interfacial traps. The initial bulk charge density, ρ_0 , is generated in the region $x > d$, and the high absorbance of HAT5 at 319 nm allows us to assume that all the light is absorbed over a length that is much less than a sample's thickness. Assuming linear absorption and that the recombination rates for charges generated at the interface are the same as those generated within the bulk, we may use the Beer-Lambert law to associate the initial number of holes with the average length of the interfacial trapping region

$$d = \frac{1}{\alpha} \ln \left(\frac{n_{s0}}{n_0} + 1 \right), \quad (22)$$

where α is the absorption coefficient for HAT5 at 319 nm, n_{s0} is the number of charges generated within the interface region, and n_0 is the number of charges generated within the bulk region.

The average length of interfacial traps as a function of applied field for sample III was difficult to resolve due to the trapping region being very short. Sample II, however, had

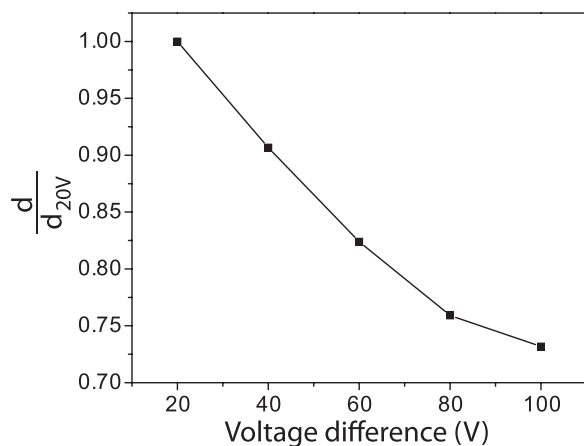


FIG. 12. Sample II's average length of interfacial traps as a function of the applied voltage at 85 °C. Here, d_{20V} is the average length of the interfacial traps at 20 V.

very large values for n_{s0}/n_0 , which corresponds to broad interfacial traps. As shown in Fig. 12, the length of the trapping region decreases as the applied field is increased. Thus, the increased potential difference significantly reduces the effects of interfacial trapping of samples with broad interfacial traps. For sample II, we observe that the change in the average interfacial trapping lengths decreases by more than 25% from 20 V to 100 V. The length of broad trapping regions is speculated to decrease when the voltage slope is increased as observed in the diagram of Fig. 7.

VI. CONCLUSIONS

We have shown that HAT5 samples, aged under ambient conditions for 10 years, have a slow increase in photocurrent, which is in contrast to the pristine samples. Experimental evidence from wavelength dependent measurements and the three-state charge-trapping model are in good agreement with the hypothesis that low-energy traps form primarily near the interfaces. Delayed-pulse TOF measurements of the positive charge carriers confirm that interfacial traps are not formed by mobile ion build-up at the interfaces; however, MALDI-TOF studies show molecular impurities in aged HAT5 that offer the most reasonable explanation for these interfacial traps. The chemically different impurity does not affect the bulk mobility but instead forms well-defined interfacial traps in connection to the Schottky barrier.^{52,53}

With a phenomenological three-state model used in conjunction with the continuity equation, we conclude that the transient behavior reflects competitions among trapping, intermediate, and bulk reservoir states. This model has been shown to be computationally efficient in reproducing the observed transients, where the method of competing collection/release rates of the system of charge carriers describes the slow non-exponential rise of the photocurrents observed in aged HAT5.

The impurities do not appear to have a significant effect on the mobility within the sample-to-sample uncertainty. Note that only a small amount of impurity in the material was detected with mass spectrometry while there was a significant amount of trapped charges at the interface.

Therefore, we also conclude that charge carrier TOF can be an exquisitely sensitive method to determine the purity of some semiconducting liquid crystals.

ACKNOWLEDGMENTS

N.J.D., M.S.P., and K.D.S. thank the National Science Foundation, Grant No. OISE-1243313, for supporting this project. R.M. and E.B.P. thank the Case Western Reserve University College of Arts and Sciences.

- ¹D. Adam, F. Closs, T. Frey, D. Funhoff, D. Haarer, H. Ringsdorf, P. Schuhmacher, and K. Siemensmeyer, "Transient photoconductivity in a discotic liquid crystal," *Phys. Rev. Lett.* **70**, 457–460 (1993).
- ²R. J. Bushby and O. R. Lozman, "Discotic liquid crystals," *Curr. Opin. Solid State Mater. Sci.* **6**, 569–578 (2002).
- ³S. Sergeev, W. Pisula, and Y. H. Geerts, "Discotic liquid crystals: a new generation of organic semiconductors," *Chem. Soc. Rev.* **36**, 1902–1929 (2007).
- ⁴J. Billard, J. C. Dubois, N. H. Tinh, and A. Zann, "Mesophase of disc-like molecules," *Nouv. J. Chim.* **2**, 535–540 (1978).
- ⁵V. Lemaire, D. A. d. S. Filho, V. Coropceanu, M. Lehmann, Y. Geerts, J. Piris, M. G. Debije, A. M. v. d. Craats, K. Senthilkumar, L. D. A. Siebbeles, J. M. Warman, J.-L. Brédas, and J. Cornil, "Charge transport properties in discotic liquid crystals: A quantum-chemical insight into structure-property relationships," *J. Am. Chem. Soc.* **126**, 3271–3279 (2004).
- ⁶*Self-Organized Organic Semiconductors: From Materials to Device Applications*, edited by Q. Li (John Wiley & Sons, Hoboken, NJ, 2010).
- ⁷V. Duzhko, A. Semyonov, R. J. Twieg, and K. D. Singer, "Correlated polaron transport in a quasi-one-dimensional liquid crystal," *Phys. Rev. B* **73**, 064201 (2006).
- ⁸M. Pope and C. E. Swenberg, *Electronic Processes in Organic Crystals* (Clarendon, Oxford, 1982), p. 337.
- ⁹N. Boden, R. J. Bushby, J. Clements, B. Movaghar, K. J. Donovan, and T. Kreouzis, "Mechanism of charge transport in discotic liquid crystals," *Phys. Rev. B* **52**, 13274–13280 (1995).
- ¹⁰T. Holstein, "Studies of polaron motion. Part I. The molecular-crystal model," *Ann. Phys.* **8**, 325–342 (1959).
- ¹¹T. Holstein, "Studies of polaron motion. Part I. The 'small' polaron," *Ann. Phys.* **8**, 343–389 (1959).
- ¹²S. T. Martin, H. Herrmann, W. Choi, and M. R. Hoffmann, "Time-resolved microwave conductivity. Part I. TiO₂ photoreactivity and size quantization," *J. Chem. Soc. Faraday Trans.* **90**, 3315–3322 (1994).
- ¹³J. M. Warman, M. P. de Haas, S. W. F. M. Van Hovell tot Westerflier, J. J. M. Binsma, and Z. I. Kolar, "Electronic processes in semiconductor materials studied by nanosecond time-resolved microwave conductivity. 1. Cadmium sulfide macroscopic crystal," *J. Phys. Chem.* **93**, 5895–5899 (1989).
- ¹⁴A. M. van de Craats, J. M. Warman, M. P. de Haas, D. Adam, J. Simmerer, D. Haarer, and P. Schuhmacher, "The mobility of charge carriers in all four phases of the columnar discotic material hexakis(hexylthio)triphenylene: Combined TOF and PR-TRMC results," *Adv. Mater.* **8**, 823–826 (1996).
- ¹⁵A. M. van de Craats, M. P. de Haas, and J. M. Warman, "Charge carrier mobilities in the crystalline solid and discotic mesophases of hexakis-hexylthio and hexakis-hexyloxy triphenylene," *Synth. Met.* **86**, 2125–2126 (1997).
- ¹⁶P. N. Murgatroyd, "Theory of space-charge-limited current enhanced by Frenkel effect," *J. Phys. D: Appl. Phys.* **3**, 151–156 (1970).
- ¹⁷C. Tanase, P. W. M. Blom, and D. M. de Leeuw, "Origin of the enhanced space-charge-limited current in poly(p-phenylene vinylene)," *Phys. Rev. B* **70**, 193202 (2004).
- ¹⁸J. M. Montero, J. Bisquert, G. Garcia-Belmonte, E. M. Barea, and H. J. Bolink, "Trap-limited mobility in space-charge limited current in organic layers," *Org. Electron.* **10**, 305–312 (2009).
- ¹⁹H. Li, L. Duan, D. Zhang, G. Dong, J. Qiao, L. Wang, and Y. Qiu, "Relationship between mobilities from time-of-flight and dark-injection space-charge-limited current measurements for organic semiconductors: A Monte Carlo study," *J. Phys. Chem. C* **118**, 6052–6058 (2014).
- ²⁰H. Zhang and J. Hanna, "Photocarrier generation in smectic phenyl-naphthalene liquid crystalline photoconductor," *J. Phys. Chem. B* **103**, 7429–7434 (1999).

- ²¹I. Shiyankovskaya, K. D. Singer, V. Percec, T. K. Bera, Y. Miura, and M. Glodde, "Charge transport in hexagonal columnar liquid crystals self-organized from supramolecular cylinders based on acene-functionalized dendrons," *Phys. Rev. B* **67**, 035204 (2003).
- ²²B. Ellman, H. Nene, A. N. Semyonov, and R. J. Twieg, "High mobility, low dispersion hole transport in 1,4-diiodobenzene," *Adv. Mater.* **18**, 2284–2288 (2006).
- ²³C. Pokhrel, N. Shakya, S. Purtee, B. Ellman, A. N. Semyonov, and R. J. Twieg, "Effect of mobile ions on charge mobility measurements," *J. Appl. Phys.* **101**, 103706 (2007).
- ²⁴H. Li, L. Duan, C. Li, L. Wang, and Y. Qiu, "Transient space-charge-perturbed currents in organic materials: A Monte Carlo study," *Org. Electron.* **15**, 524–530 (2014).
- ²⁵A. Ohno, J. Hanna, and D. H. Dunlap, "Analysis of trap distribution using time-of-flight spectroscopy," *Jpn. J. Appl. Phys., Part 1* **47**, 1079–1088 (2008).
- ²⁶H. Iino, J. Hanna, D. Haarer, and R. J. Bushby, "Fast electron transport in discotic columnar phases of triphenylene derivatives," *Jpn. J. Appl. Phys., Part 1* **45**, 430–433 (2006).
- ²⁷H. Zhang and J. Hanna, "Electrode effect on photohole generation in smectic phenylanthracene liquid crystalline photoconductor," *J. Appl. Phys.* **88**, 270–277 (2000).
- ²⁸See EPAPS Document No. E-PRBMDO-73-032606 for a detailed procedure of HAT5 fabrication. The document can be found on the website of the American Institute of Physics (<http://aip.org>).
- ²⁹H. Iino, J. Hanna, D. Haarer, and R. J. Bushby, "Electronic and ionic carrier transport in discotic liquid crystalline photoconductor," *Phys. Rev. B* **72**, 193203 (2005).
- ³⁰H. Scher and E. W. Montroll, "Anomalous transit-time dispersion in amorphous solids," *Phys. Rev. B* **12**, 2455–2477 (1975).
- ³¹C. P. Pokhrel, "Crystal growth and charge carrier transport in liquid crystals and other novel organic semiconductors," Ph.D. thesis (Kent State University, 2009).
- ³²We also tested oxidation as the route of degradation by adding water to a HAT5/chloroform solution and exposing the solid HAT5 to ozone. In both cases, the HAT5 yellowed in the visible spectrum and a new species appeared with a molecular weight of $574 m/Z$, which is not present in the aged HAT5 material.
- ³³J. Noolandi, "Multiple-trapping model of anomalous transit-time dispersion in $a - Se$," *Phys. Rev. B* **16**, 4466–4473 (1977).
- ³⁴J. Noolandi, "Equivalence of multiple-trapping model and time-dependent random walk," *Phys. Rev. B* **16**, 4474–4479 (1977).
- ³⁵F. W. Schmidlin, "Theory of trap-controlled transient photoconduction," *Phys. Rev. B* **16**, 2362–2385 (1977).
- ³⁶J. Rybicki and M. Chybicki, "Multiple-trapping transient currents in thin insulating layers with spatially nonhomogeneous trap distribution," *J. Phys.: Condens. Matter* **1**, 4623–4634 (1989).
- ³⁷A. Pecchia, O. R. Lozman, B. Movaghar, N. Boden, R. J. Bushby, K. J. Donovan, and T. Kreouzis, "Photoconductive transients and one-dimensional charge carrier dynamics in discotic liquid crystals," *Phys. Rev. B* **65**, 104204 (2002).
- ³⁸N. Rappaport, O. Solomesch, and N. Tessler, "The mobility spatial distribution function: Turn-on dynamics of polymer photocells," *J. Appl. Phys.* **99**, 064507 (2006).
- ³⁹M. Tessler, Y. Preezant, N. Rappaport, and Y. Roichman, "Charge transport in disordered organic materials and its relevance to thin-film devices: A tutorial review," *Adv. Mater.* **21**, 2741–2761 (2009).
- ⁴⁰P. M. Borsenberger, L. T. Pautmeier, and H. Bassler, "Nondispersive-to-dispersive charge-transport transition in disordered molecular solids," *Phys. Rev. B* **46**, 12145–12153 (1992).
- ⁴¹H. Bässler, "Charge transport in disordered organic photoconductors a Monte Carlo simulation study," *Phys. Status Solidi B* **175**, 15–56 (1993).
- ⁴²B. Hartenstein and H. Bässler, "Transport energy for hopping in a Gaussian density of states distribution," *J. Non-Cryst. Solids* **190**, 112–116 (1995).
- ⁴³A. Picos-Vega and O. Zelaya-Angel, "Monte Carlo simulation of charge-trapped effects on dispersive electronic transient transport," *Phys. Rev. B* **58**, 14845 (1998).
- ⁴⁴A. Ohno, H. Iino, K. Kurotaki, A. Haruyama, J. Hanna, and D. H. Dunlap, "Analysis of trap distribution for smectic liquid crystals using time of flight spectroscopy," *Proc. SPIE* **5937**, 59371X (2005).
- ⁴⁵D. K. D. Gupta and K. Joyner, "Anomalous photo-induced current transients in polyethylene," *J. Phys. D* **5**, 1368–1373 (1972).
- ⁴⁶C. G. Van de Walle, "Stretched-exponential relaxation modeled without invoking statistical distributions," *Phys. Rev. B* **53**, 11292–11295 (1996).
- ⁴⁷R. M. Corless, G. H. Gonnet, D. E. G. Hare, D. J. Jeffrey, and D. E. Knuth, "On the Lambert W function," *Adv. Comput. Math.* **5**, 329–359 (1996).
- ⁴⁸R. Courant, E. Isaacson, and M. Rees, "On the solution of nonlinear hyperbolic differential equations by finite differences," *Commun. Pure Appl. Math.* **5**, 243–255 (1952).
- ⁴⁹R. E. Ewing and H. Wang, "A summary of numerical methods for time-dependent advection-dominated partial differential equations," *J. Comput. Appl. Math.* **128**, 423–445 (2001).
- ⁵⁰The time spent calculating the nonlinear fits depends on the number of time steps and number of iterations necessary to find a convergent solution, where the latter varies significantly.
- ⁵¹W. Wang, X. Liu, and J. Pu, "Electric-field response of discotic hexabenzocoronene (HBC) liquid crystals," *Molecules* **16**, 9101–9108 (2011).
- ⁵²V. B. Bondarenko, A. V. Filimonova, and E. Y. Koroleva, "The Schottky barrier at homogeneous impurity distribution in a semiconductor," *J. Surf. Invest. X-Ray, Synchrotron Neutron Tech.* **4**, 859–861 (2010).
- ⁵³R. Pal, V. Gopal, P. K. Chaudhury, B. L. Sharma, P. K. Basu, O. P. Agnihotri, and V. Kumar, "Study of interface traps from transient photoconductive decay measurements in passivated HgCdTe," *J. Electron. Mater.* **30**, 103–108 (2001).